communications materials

ARTICLE

https://doi.org/10.1038/s43246-022-00314-7 OPEN

Point-defect avalanches mediate grain boundary diffusion

Ian Chesser [1]✉ & Yuri Mishin [1]✉

Grain boundary diffusion in polycrystalline materials is a physical phenomenon of great fundamental interest and practical significance. Although accelerated atomic transport along grain boundaries has been known for decades, atomic-level understanding of diffusion mechanisms remains poor. Previous atomistic simulations focused on low temperatures where the grain boundary structure is ordered or high temperatures where it is highly disordered. Here, we conduct molecular dynamics simulations of grain boundary diffusion at intermediate temperatures most relevant to applications. A surprising result of this work is the observation of intermittent GB diffusion behavior and its strong system-size dependence unseen in previous work. Both effects are found to originate from thermally activated point-defect avalanches. We identify the length and time scales of the avalanches and link their formation to dynamic heterogeneity in partially disordered systems. Our findings have implications for future computer modeling of grain boundary diffusion and mass transport in nano-scale materials.

[1] Department of Physics and Astronomy, MSN 3F3, George Mason University, Fairfax, VA 22030, USA. ✉email: ichesser@gmu.edu; ymishin@gmu.edu

Most technological materials are composed of differently oriented crystallites (grains) separated by a network of grain boundaries (GBs)[1]. Atomic transport along GBs is known to be much faster than in the perfect lattice[2]. This short-circuit GB diffusion controls many processes in structural and functional materials, including microstructure development, phase transformations, and high-temperature modes of plastic deformation and fracture[1,2]. In addition to the practical significance, GB diffusion is a phenomenon of great fundamental interest. Being in a frustrated state squeezed between misoriented crystals, the quasi-two-dimensional GB structure represents a unique state of matter transitional between ordered and disordered. Due to this structural complexity, the current understanding of GB diffusion mechanisms remains very limited. Experiments can only measure numerical values of GB diffusion coefficients but provide little information about the microscopic mechanisms. Hence, practically all existing knowledge about GB diffusion mechanisms comes from atomistic computer simulations[3].

Previous simulations have only addressed two limiting cases of relatively low and relatively high temperatures. It is now established that at low temperatures ($T \ll T_m$, where T_m is the melting point), GBs support both vacancies and interstitials, which can exist in a variety of structural forms, have strongly site-dependent but on average lower formation energies than in the lattice, and can contribute equally to GB diffusion[4–7]. GB atoms can diffuse by a variety of different but predominantly collective mechanisms, typically in the form of a chain of highly coordinated displacements that can be open-ended (string) or looped (ring). In the other limit, when temperature approaches the bulk melting point, the GB structure becomes highly disordered. Some GBs premelt by transforming into a liquid-like layer near T_m[6–8]. The notion of individual point defects breaks down, but the diffusion mechanisms remain collective and closely resemble those in disordered bulk systems such as supercooled liquids, glasses, superheated crystals and crystalline super-ionic materials[9–13]. Accordingly, the statistical methods developed for the characterization of atomic dynamics in disordered bulk systems were successfully applied to study diffusion mechanisms in disordered GBs[7,8]. Such studies revealed a remarkable similarity between the two types of systems, including the existence of string-like diffusion mechanisms and the dynamic heterogeneity occurring on multiple length and time scales.

Little is known about GB diffusion mechanisms at intermediate temperatures, at which the GB structure is not liquid-like but rather retains a significant degree of structural order. It is presently unknown if the concepts of dynamic heterogeneity and dynamic facilitation developed for disordered systems can be applied to such boundaries. If they can, the length and time scales involved in the heterogeneous dynamics remain unexplored. It should also be noted that the intermediate temperatures are more relevant to the service conditions of many technological materials than the two limiting cases mentioned above.

This work aims to fill this knowledge gap by studying the diffusion mechanisms in metallic GBs at intermediate temperatures. A surprising outcome of the study is the observation of a strongly intermittent diffusion behavior and its system-size dependence unseen in previous work. We show that both effects originate from an intermittent, avalanche-type generation of point defects causing spontaneous bursts of GB diffusivity. We carefully characterize the length and time scales of the avalanches and show that they fully explain the observed intermittent diffusion behavior and its size dependence. We discuss possible implications of our findings for the computer modeling of GB diffusion and for atomic transport in nanoscale systems.

Table 1 Crystallography and 0 K energies of Al GBs.

GB description	x	y	z	γ (mJ/m^2)
Σ3 ⟨110⟩ tilt 70.5°	[−1, 1, 1] [1, −1, −1]	[0, 1, −1] [0, −1, 1]	[2, 1, 1] [2, 1, 1]	418
Σ17 ⟨100⟩ tilt 61.9°	[5, −3, 0] [−5, 3, 0]	[0, 0, −1] [0, 0, 1]	[3, 5, 0] [3, 5, 0]	488
Σ85 {100} twist 8.8°	[−1, 13, 0] [1, 13, 0]	[13, 1, 0] [−13, 1, 0]	[0, 0, 1] [0, 0, 1]	306
HAAI {100}||{111}	[1, 1, 0] [1, 1, −2]	[1, −1, 0] [1, −1, 0]	[0, 0, 1] [1, 1, 1]	306

The Cartesian *x*, *y* and *z* axes are aligned with edges of the rectangular simulation box. The GB plane is normal to the *z*-direction. For each GB, the two lines indicate crystallographic directions parallel to the Cartesian axes in the upper and lower grain. The GB energy (γ) was computed with the interatomic potential from Ref. [15].

Four different GBs were selected for this study (Table 1). These four boundaries represent diverse GB crystallographies, symmetries, and atomic structures. The primary material considered is Face Centered Cubic (FCC) Al, though main results are reproduced in FCC Ni and Body Centered Cubic (BCC) Fe GBs. Most of the results reported below are for the Σ3 and Σ17 GBs, with two remaining boundaries left for cross-checking. We note that both the Σ3 incoherent twin GB and the high-angle asymmetric incommensurate (HAAI boundary) have relatively low energies and are common in polycrystalline Al[14]. To model GB diffusion, we use classical molecular dynamics (MD) with atomic interactions described with the interatomic potential[15] referred to as Al-M. To demonstrate that our results are not a specific feature of a particular potential, some of the simulations are repeated with two other Al potentials. In all cases, the results are well-consistent with those obtained with the Al-M potential for the Σ3 and Σ17 GBs, confirming the robustness of our conclusions.

Results

0 K GB structure. The Σ3 and Σ17 GB structures optimized with the Al-M potential are shown in Fig. 1a, b. The GB construction and optimization protocol is explained in the Methods section. The Σ3 GB, also known as incoherent twin boundary, comprises asymmetric kite-shaped structural units. This structure closely matches the high-resolution transmission electron microscopy observations[16,17] and prior simulations[18]. Its asymmetry arises from a small shift of the upper grain relative to the lower along the ⟨111⟩ axis (*x*-direction in the sample frame), whose magnitude (0.7 A) is close to the experimental value (0.66 ± 0.07Å)[17]). This boundary also has a symmetric structure (zero shift)[17,19], but the latter has a higher energy. We thus use the asymmetric structure for the diffusion simulations. The Σ17 GB has a zig-zag structure with the kite-unit spacing (0.59 nm) and energy consistent with prior simulations[20]. This boundary was previously used to study premelting diffusion mechanisms in copper[7].

Diffusion coefficients. Self-diffusion coefficients in the Σ3 and Σ17 GBs were extracted from MD trajectories using the Einstein relation as detailed in Methods. The results are summarized in the Arrhenius diagram in Fig. 1c. For comparison, the diagram also shows the diffusion coefficients in liquid Al computed in this work and the diffusion coefficients in FCC Al taken from the literature. In agreement with prior work[6], the GB diffusion coefficients are intermediate between those in the supercooled liquid and in the perfect crystal. Both GBs exhibit diffusion anisotropy with faster diffusion along the tilt axis (*y*-axis) than normal to it (*x*-axis). Diffusion in the Σ3 GB exhibits a larger

degree of anisotropy and is over an order of magnitude slower than diffusion in the Σ17 GB (except close to the melting temperature where the two diffusivities tend to converge). This behavior correlates with the lower energy of the Σ3 GB (418 mJ/m^2) relative to the Σ17 GB (488 mJ/m^2)[5,6].

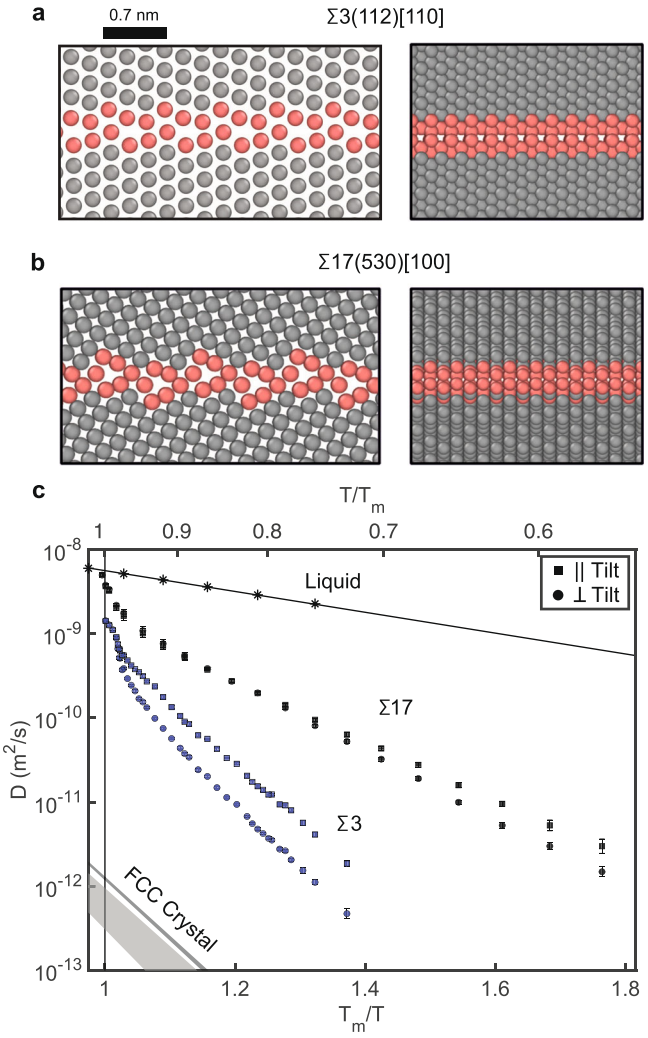

Fig. 1 Atomic structures and diffusion coefficients for the Al Σ3 and Σ17 GBs. a, **b** The optimized GB structures as viewed parallel (left column) and normal (right column) to the tilt axis. Atoms identified with perfect FCC coordination via common neighbor analysis are colored grey and all other atoms are colored red. **c** Arrhenius diagram of GB diffusion coefficients parallel ($D_{||}$) and perpendicular ($D_{\perp}$) to the tilt axis. The vertical line indicates the melting point predicted by the interatomic potential. Shown for comparison are the computed diffusivities in liquid Al and the experimental (dashed stripe)[53,54] and computed (lower stripe)[21] literature data for self-diffusion in FCC Al.

Below the homologous temperature of $0.9T_m$ ($T_m = 929$ K being the Al melting point predicted by the Al-M potential), the GB diffusion coefficients follow the Arrhenius relation

$$D_i = D_{0,i} \exp\left(-\frac{E_i}{k_B T}\right), \quad (1)$$

where the index i refers to the directions parallel (||) or normal (⊥) to the tilt axis, $D_{0,i}$ is the entropic prefactor, E_i is the activation energy of diffusion, and k_B is Boltzmann's constant. Table 2 summarizes the Arrhenius parameters for each GB obtained by fitting Eq. (1) to the data below $0.9T_m$. For the Σ3 GB, the average activation energy (1.38 eV) is significantly higher than for the Σ17 GB (0.77 eV) and comparable to the literature data for lattice diffusion (1.25-1.45 eV)[21]. At high temperatures, a premelting regime is observed in both GBs as evident from the rapid increase in the diffusivity with temperature. The Σ17 GB fully premelts and its diffusivity comes close to that in liquid Al near T_m, which is consistent with previous work on this GB in copper[6,20,22]. The Σ3 GB also premelts, but its diffusivity remains below the bulk liquid diffusivity. This work is focused on diffusion at intermediate temperatures $T < 0.8T_m$ ($T < 750$ K), at which both GBs are relatively flat and immobile on the MD timescales. This allows us to cleanly analyze the diffusion mechanisms without the added complications of GB roughening, migration, or premelting.

Avalanche-like diffusion mechanisms. Our first key observation is the significant intermittency of GB diffusion at the intermediate temperatures. The effect is illustrated in Fig. 2a where we plot the mean-square displacement (MSD) of atoms in the Σ3 GB core as a function of time. The remarkable feature of the plot is the slope fluctuations with stochastic switches between nearly horizontal and large-slope portions. The zig-zag shape of this plot points to the existence of two dynamic regimes with a very small and a relatively large GB diffusivity. We refer to the plateaus of the diffusivity as the locked states and to the surges of diffusion as avalanches. The times at which the avalanches nucleate correspond to abrupt increases in the number of mobile atoms in the GB core, as illustrated in Fig. 2b. In contrast, during the locked periods, most GB atoms remain immobile; only a few atoms execute jumps, usually in the form of small rings of highly correlated displacements (Fig. 2c).

The diffusivity bursts are dynamic signatures of the avalanches, but they also produce a structural signature. Each avalanche period is accompanied by a drastically increased point defect activity in the GB core and thus a temporary decrease in the structural order. An avalanche triggers a massive formation of vacancies and interstitials, which occur in almost equal amounts. Comparison of Figs. 2a and 3a shows that the numbers of

Table 2 Activation energies (E) and prefactors (D_0) for self diffusion.

GB description	Direction	E (eV)	D_0 (m^2/s)
Σ3 ⟨110⟩ tilt 70.5°	|| tilt axis	1.31 ± 0.03	(3.89 ± 7.8) × 10^{-3}
	⊥ tilt axis	1.45 ± 0.03	(1.17 ± 2.24) × 10^{-2}
Σ17 ⟨100⟩ tilt 61.9°	|| tilt axis	0.72 ± 0.01	(5.53 ± 1.59) × 10^{-6}
	⊥ tilt axis	0.81 ± 0.01	(2.09 ± 0.74) × 10^{-5}
Supercooled liquid		0.227 ± 0.001	(9.69 ± 0.24) × 10^{-8}
FCC crystal:			
Experiment[53]		1.32	1.79 × 10^{-5}
DFT calculations[21]		1.25 – 1.35	5.42 × 10^{-6} – 2.42 × 10^{-5}

The reference data for diffusion in FCC Al is taken from experiments[53] and first-principles density functional theory (DFT) calculations with several different DFT functionals[21].

vacancies and interstitials in the GB core strongly correlate not only with each other but also with the occurrence of locked and avalanche time periods. The fluctuating point defect populations also correlate with the total number of mobile atoms (Fig. 3a, c), confirming that GB diffusion occurs by defect-mediated mechanisms. At 700 K, a typical avalanche creates hundreds of point defects and activates thousands of mobile atoms.

The questions then arise: how does an avalanche begin, and how does it end? Careful structural analysis (see Methods) reveals that a typical avalanche starts with the formation of an interstitial atom in the GB core that hops multiple times (on the ps timescale) before pushing a regular atom out of its preferred site (Fig. 3b). This event triggers a cascade of collective structural excitations with a string-like character in which multiple atoms move simultaneously in the same direction. A string-like excitation can be viewed as an extended Frenkel pair in which the leading atom has an interstitial character (associated with local compression) and the trailing atom has a vacancy character (associated with local tension). This interpretation is confirmed by analyzing the free volume distribution in the population of mobile atoms (see Supplementary Fig. 1). Importantly, the avalanches involve the facilitated dynamics[23,24] of the multiple Frenkel pairs and neighboring string-like excitations. Namely, a collective atomic displacement at one location triggers nearby diffusive events, creating a positive feedback for further propagation of the atomic displacement field that rapidly grows in size into a full-fledged avalanche. As the point-defect population grows, so does the probability of their mutual recombination. Eventually, a bifurcation point is reached at which the dynamics switch to a recombination regime. We hypothesize that the locked states arise from spontaneous switches of the diffusion process from the multiplication to the recombination regime. Self-annihilation of point defects across the periodic boundary conditions can also play a role.

Our second key finding is that the intermittent behavior of GB diffusion is system-size dependent on the ~10 nm length scale.

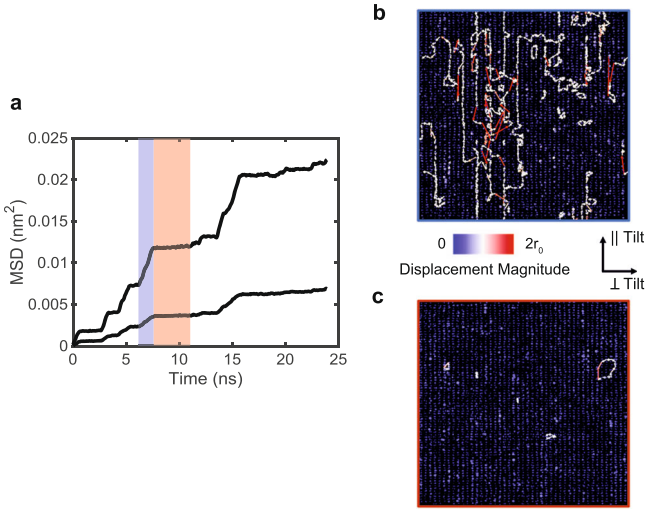

Fig. 2 Example of intermittent diffusion at intermediate temperatures. **a** Atomic MSD as a function of time at 710 K (0.77 T_m) for the Σ3 GB for a typical GB cross-section (10 nm × 10 nm). Typical atomic displacement diagrams during the **b** avalanche and **c** locked time periods corresponding to the blue and red regions in (**a**). The arrows represent net displacements during time intervals of 1.2 ns and 3 ns and are colored by the displacement magnitude. The scale bar has units of first nearest neighbor distance r_0. Note the enhanced atomic mobility in the avalanche regime and only a few displaced atoms in the locked regime.

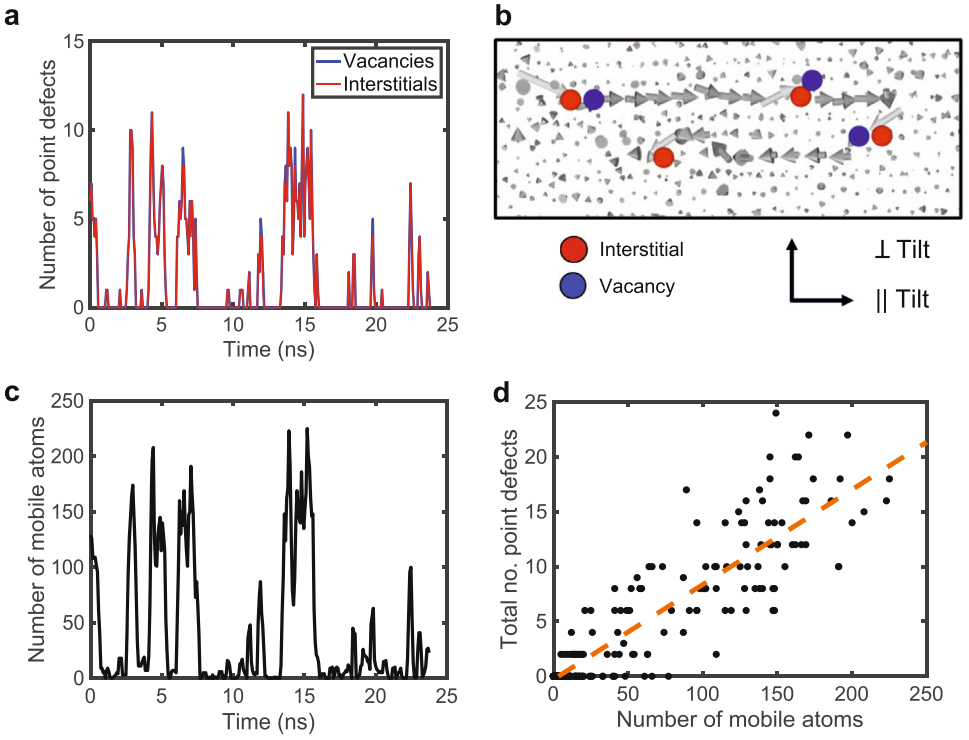

Fig. 3 Point defect signatures of avalanche-like diffusion. **a** Peaks in the numbers of vacancies and interstitials correlate with the locked and avalanche time periods seen in Fig. 2a. **b** A typical collective diffusion event involves the formation and multiplication of Frenkel pairs. The arrows represent string-like displacements during the time interval $\Delta t = 80$ ps and colored in dark grey and light grey for displacements smaller and larger than the first-neighbor distance r_0. **c** Peaks in the number of mobile atoms also correlate with the locked and avalanche time periods. **d** Correlation between the point-defect population and the number of mobile atoms in the GB core with the correlation factor of $R^2 = 0.83$.

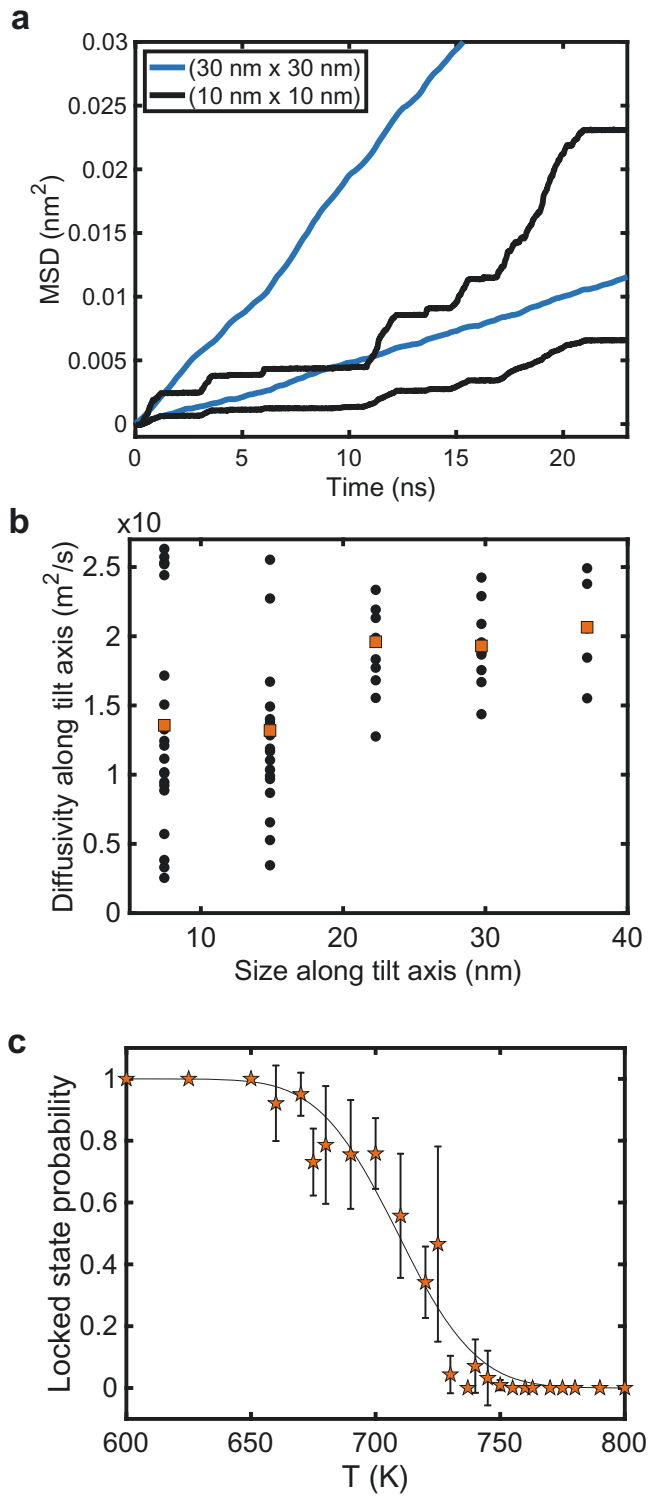

Fig. 4 Finite size effects of diffusion and temperature dependence. **a** Atomic MSD versus time at the temperature of 700 K (0.75 T_m) for the (10 nm × 10 nm) and (30 nm × 30 nm) GB cross-sections for the Al Σ3 GB. Note that the diffusion intermittency disappears with increasing cross-section. **b** Size dependence of GB diffusivity for several different cross-sections with a fixed 13 nm size perpendicular to the tilt axis and a varied size from 6 nm to 38 nm along the tilt axis. The points represent independent MD runs with different velocity seeds. The red points represent the average values. **c** Locked-state probability (fraction of plateau portions in (**a**)) as a measure of intermittency plotted as a function of temperature. The error bars are obtained by using up to ten velocity seeds at each temperature. The sigmoidal fit is only meant to guide the eye. Note the suppression of intermittency with increasing temperature.

This was demonstrated by increasing the GB cross-section and remeasuring the diffusion coefficients and the MSD curves. In the example shown in Fig. 4a, the initial zig-zag shape of the MSD curves is replaced by linear functions when the cross-section is increased from (10 nm × 10 nm) to (30 nm × 30 nm). In a more systematic test, the GB cross-section in the direction parallel to the tilt axis was increased incrementally while keeping the size normal to the tilt axis fixed. For each cross-section, the diffusivity was measured several times with different velocity seeds as shown in Fig. 4b. The scatter of the points at each cross-section is a measure of the intermittent diffusion behavior. The plot clearly shows that the scatter decreases with increasing GB size. (The average diffusivity values seem to increase with the size, but this trend does not pass statistical significance tests.) The probability of locked states can also be used as a measure of intermittency. The plot Fig. 4c shows that, for a fixed (10 nm × 10 nm) cross-section, the intermittency decreases with increasing temperature and vanishes at about 750 K. These tests demonstrate that the intermittent behavior of GB diffusion exists in a particular temperature-size domain and disappears at high temperatures and/or large GB sizes.

We posit that both phenomena, the GB diffusion intermittency and its size dependence, have the same physical origin: the finite size of the mobile atom clusters generated by the point-defect avalanches. In a large GB area, multiple avalanches can form at different moments at random locations. The measured diffusion coefficient then represents the atomic mobility averaged over multiple avalanches and exhibits a smooth and size-independent behavior. If the GB size is less than or comparable to the avalanche size, the boundary conditions truncate the mobile cluster to the GB size. Each mobility surge then quickly spreads over the entire GB area and later stops across the entire GB area, causing the on-and-off behavior seen in Figs. 3a and 4a. Due to the anisotropy of GB structure, the intermittency condition can be met when the mobile cluster size becomes comparable to the GB linear dimension in at least one direction. The disappearance of the diffusion intermittency at high temperatures is explained by a decrease in the mobile cluster size with temperature.

To provide mechanistic support to this explanation, we have analyzed the dynamic length scales of the GB diffusion in more detail. We find that the measures of dynamic length scales used in previous work[8,11] predict lengths that are too small in magnitude to explain the observed diffusion intermittency. For example, the average (1.4 nm) and maximum (7 nm) string lengths computed for the Σ3 GB at 700 K by the standard string-like segmentation method (see Methods) are smaller than the observed ~10 nm system-size effect. A method capturing the length scale of the entire avalanche region was required.

As stated above, the avalanches exist due to the dynamic facilitation of collective atomic displacements, in which a local excitation spreads in a self-catalytic manner by increasing the probability of atomic displacements in neighboring regions. Facilitated dynamics can be conveniently visualized using space-time diagrams[23]. To construct such a diagram, displacement fields corresponding to a fixed time interval are stacked together along the time axis and viewed in a space-time cross-section (Fig. 5a, b). We note that in Fig. 5a, artistic license is taken such that the finite width of the GB core along the z direction is visible along the time axis. The diagram reveals the formation and disappearance of mobile and immobile clusters in space and time.

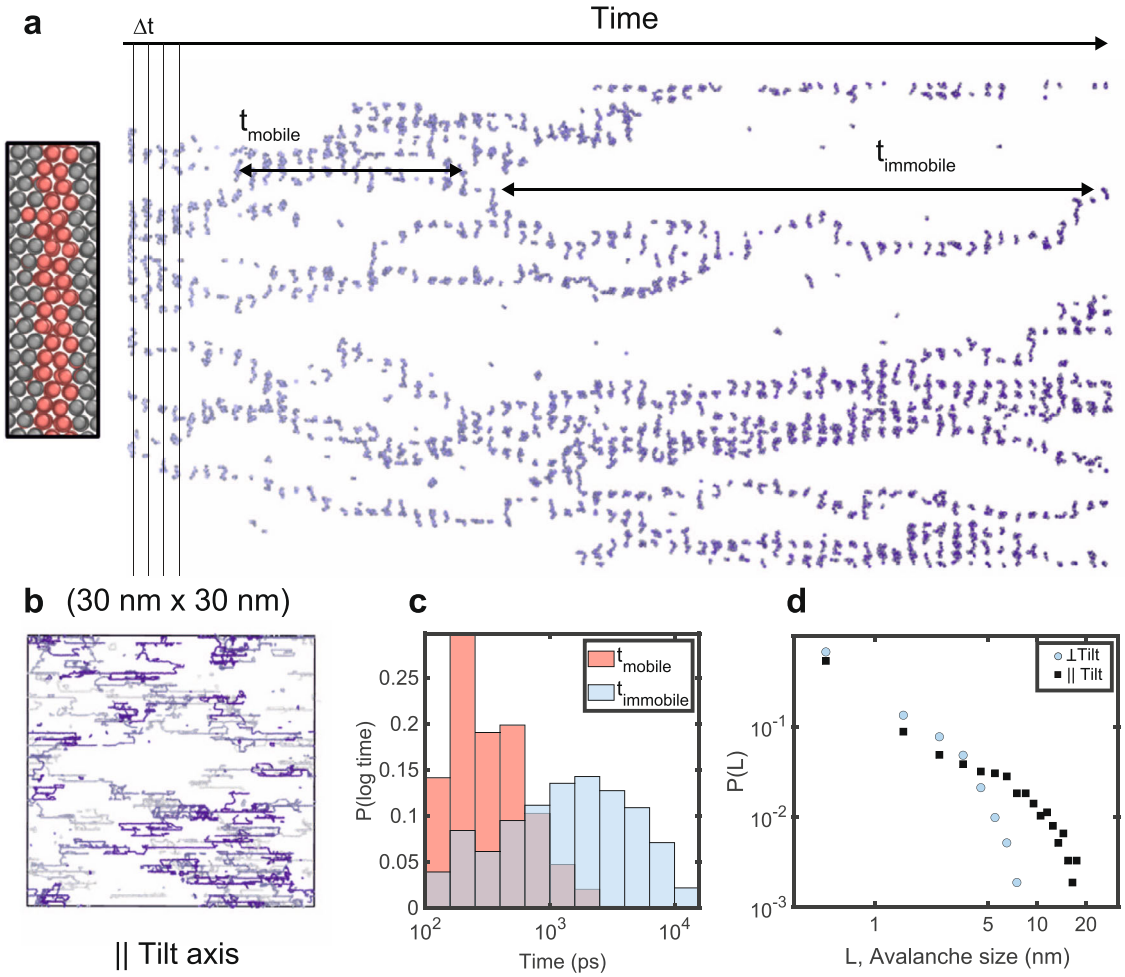

Fig. 5 Avalanche time and length scales. a Space-time atomic mobility diagram for the Σ3 GB at 700 K computed with the time interval of $\Delta t = 40$ ps and viewed perpendicular to the tilt axis. The finite temperature GB structure is shown on the left with light grey FCC atoms and red non-FCC atoms. The immobile clusters are evident as voids (or bubbles)[24] separating mobile atom trajectories. The arrows show examples of mobile and immobile cluster dimensions in time. **b** Cross section of the same diagram with all time data projected onto the GB plane. The rectangular box indicates the 6 nm scale of the GB structure shown in (**a**) relative to the GB area. **c** Probability distribution of lifetimes of mobile and immobile clusters. Note that immobile clusters persist on a longer time scale than mobile clusters. **d** Avalanche size distribution at 720 K as measured by the maximum avalanche size perpendicular and parallel to the tilt axis. The avalanches are elongated along the tilt axis and exhibit a cutoff behavior with large avalanches becoming increasingly unlikely with increasing size. Note that the cutoff size along the tilt axis is larger than 10 nm.

The GB structural units blink between on and off states corresponding to the diffusive and quiescent time periods. The branching and coalescence of diffusion trajectories on the diagram are signatures of facilitated dynamics. We have developed a space-time clustering algorithm (see Methods) that identifies the mobile and immobile clusters and measures their dimensions in space and time. The time dimensions of these clusters are associated with the lifetimes of the avalanches and locked states. As demonstrated in Fig. 5c, we find that immobile clusters have a longer average lifetime than mobile clusters. This time scale separation is a known hallmark of facilitated dynamics[23,24]. The spatial dimensions of the mobile and immobile clusters are measures of avalanche size. Figure 5d displays the avalanche size probability distribution computed for the Σ3 GB at 700 K. The plot shows that the avalanches are elongated parallel to the tilt axis (which is consistent with the diffusion anisotropy) and have a significant probability of being 5 to 15 nm in size. Over 15 percent of the mobile atoms participate in avalanches larger than 10 nm along the tilt axis. The largest avalanches contain a thousand or more atoms and have linear dimensions up to 20 nm along the tilt axis. These dimensions are well-consistent with the length scale of the system-size effect of GB diffusion (cf. Figs. 3a and 4a). That the avalanche size decreases with temperature was confirmed by the analysis shown in Supplementary Figure 2, in which the average avalanche size was estimated by the virtual system-size analysis explained in Methods.

GB character and material dependence of avalanche-like diffusion mechanisms. The intermittent behavior and its disappearance with increasing system size have been confirmed for the (100) twist and HAIC boundaries, as illustrated in Fig. 6. These boundaries are crystallographically and structurally different from the Σ3 and Σ17 GBs but exhibit the same correlation between the avalanche time periods on the MSD plots and the bursts of point-defect activity as found in the Σ3 and Σ17 GBs. These tests confirm the generic character of our main results for a wide variety of GB structures.

All simulations discussed so far utilized the Al-M interatomic potential[15]. To demonstrate further generality of our results, selected simulations were repeated with two additional Al

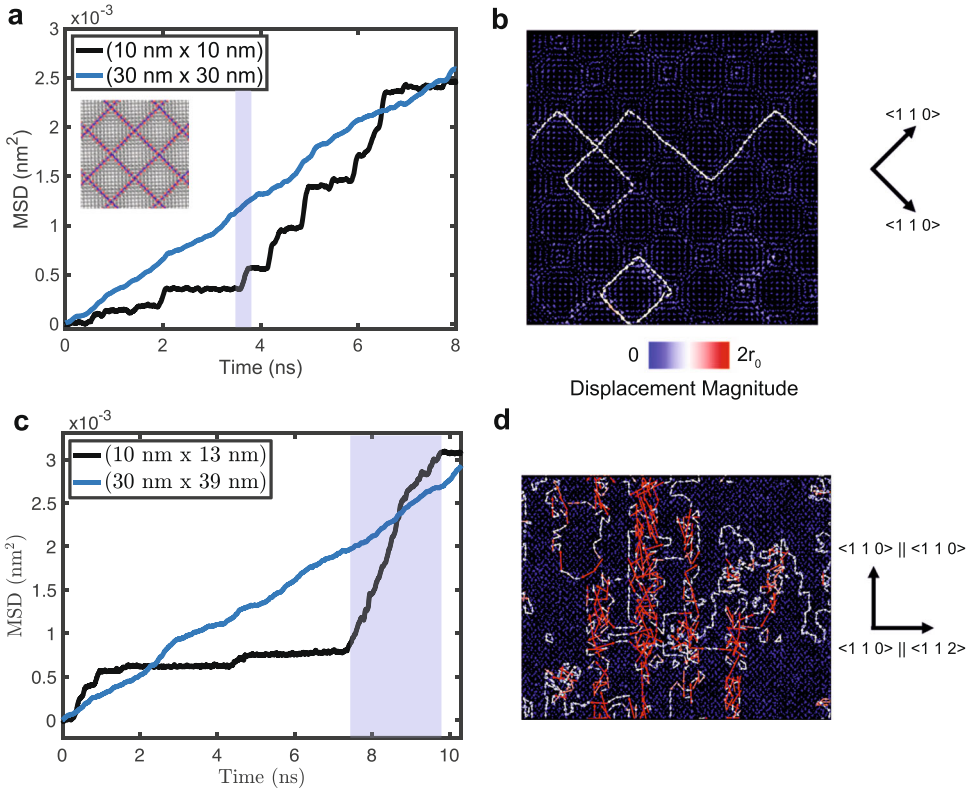

Fig. 6 Avalanche-like diffusion behavior for various GB types. Intermittent diffusion behavior in the **a**, **b** Σ85{100} low-angle twist GB at 500 K and **c**, **d** {100}||{111} HAIC GB at 700 K. The twist GB is composed of a square network of dislocations displayed in the top left corner of the MSD plot. Panels (**b**) and (**d**) are atomic displacement maps using the same color coding as in Fig. 3 and representing the avalanches shown as blue highlighted regions in (**a**) and (**c**). In (**b**), the GB structure constrains the collective atomic displacements to the dislocation cores, resulting in string-like and ring-like trajectories.

potentials and diffusion calculations were conducted for the Σ3 GB in FCC Ni and the Σ17 GB in BCC Fe (described in Supplementary Table 1) with the embedded-atom interatomic potentials developed in[25] and[26] and applied to surveys of GB properties in[27] and[28]. The additional Al potentials include the embedded-atom potential from ref. [29] (Al-99) and the recently developed physically-informed neural network (PINN) potential[30] referred to here as Al-PINN. The latter is computationally much slower than the Al-M and Al-99 potentials but gives the most accurate description of Al properties (see Supplementary Table 2 for a comparison of relevant properties).

An Arrhenius diagram summarizing the diffusion coefficients in the Σ3 and Σ17 GBs computed with the Al potentials is shown in Supplementary Fig. 3a. All three potentials display similar diffusion behaviors, with a comparable degree of diffusion anisotropy and similar temperatures of premelting. More importantly, the existence of the collective diffusion mechanisms in the Σ3 and Σ17 GBs is reproduced with all three potentials. In particular, the Al-PINN simulations predict string-like displacement geometries visually indistinguishable from those obtained with the Al-M potential. Furthermore, simulations with the Al-99 potential reveal the same type of diffusion intermittency as observed with the Al-M potential (see example in Supplementary Fig. 3b).

Size dependent diffusion intermittency on the scale of 10 nm is also observed during GB diffusion in the Σ3 GB in FCC Ni and Σ17 GB in BCC Fe at intermediate temperatures (see Supplementary Fig. 4). Collective mechanisms have previously been reported in BCC Fe GBs[31], though intermittency on such large scales has not been documented. The observation of avalanches across multiple GB structures and chemistries provides strong evidence that avalanche-mediated diffusion is generic to metallic GBs at intermediate temperatures.

Discussion

The previous paradigm of GB diffusion has been that this process is continuous in time and uniform along the GB area. Contrary to this idealistic picture, we have shown that there is a temperature-size domain in which GB diffusion is discontinuous in both time and space. For the particular GBs studied here, the time and space scales of the diffusion intermittency are several nanoseconds and several nanometers, respectively, although the exact numbers can be system-dependent. The physical origin of the GB diffusion intermittency is the dynamic heterogeneity of the diffusion process. The atomic displacements are not distributed uniformly along the boundary but cluster together into large groups of mobile atoms undergoing a collective rearrangement. Spontaneous formation of a mobile cluster is triggered by a local atomic rearrangement that spreads like an avalanche by the dynamic facilitation mechanism. The avalanche region is characterized by a drastically increased defect population and enhanced atomic mobility. If the avalanche size is comparable to the GB size in at least one direction, a spike in the GB diffusivity arises. This is the cause of the system-size dependence of GB diffusion and the reason why the size effect vanishes when the GB area is large.

To put our findings in perspective with the literature, dynamic heterogeneity has been studied for years, but mostly in disordered bulk systems such as supercooled liquids and glasses[9–11,13]. The concept of dynamic facilitation was introduced more recently[23,24,32] but again in the context of bulk disordered systems. Zhang et al.[8] have shown that GB migration and diffusion processes exhibit dynamic heterogeneity similar to that in supercooled liquids. They also observed string-like atomic displacements on time and length scales similar to those in supercooled liquids. However, their work was focused primarily on GB migration rather than diffusion. Dynamic heterogeneity and

collective diffusion mechanisms were also investigated in highly disordered, premelted copper GBs[7]. Intermittent diffusion behavior was seen in MD simulations of low-angle twist GBs, but no explanation was attempted[33]. None of the prior work[7,8,33] investigated the physical origin of the GB diffusion intermittency or studied its size effect. On the other hand, avalanche-mediated dynamics were investigated by MD simulations of several processes, such as crystallization of glasses (see, e.g,[34] and references therein), but not for GB or even bulk diffusion. It should also be noted that the avalanches during glass crystallization occur in a metastable state as the system gradually transitions to a more stable state. By contrast, the avalanches discussed in this work occur in an equilibrium system and are caused by thermal fluctuations away from equilibrium. Thus, although some of the individual components of this work pre-existed, they were expanded and integrated into a coherent mechanistic explanation of the previously unknown effects reported in this article.

One lesson from this work for future atomistic simulations is that the system size effect is important. If the GB size is comparable to or smaller than the avalanche size and the simulation time is too short, the MSD-vs-time curve can represent either an avalanche or a locked state. In either case, the GB diffusivity extracted from the Einstein relation will be far from the real value. Multiple simulations with different system sizes and diffusion times are required to ensure averaging over multiple avalanche-locked cycles to obtain the converged GB diffusivity. In experiments, a nano-scale GB can exhibit intermittent mass transport, creating an additional source of noise in electronic devices[35]. The situation can, for example, be relevant to mass diffusion and/or electromigration in conductor lines in integrated circuits. Assuming a nanosecond time scale of the avalanches, the respective fluctuation frequency could be in the GHz range[36].

In addition to the practical aspects mentioned above, this work raises many fundamental questions. In contrast to the homogeneously disordered matter such as 2D or 3D supercooled liquids and glasses, GBs are partially ordered quasi-2D systems with a tunable structure and structural anisotropy. They can support a broad spectrum of local structural excitations (defects) with diverse sizes, energetics, and geometries. The effects of this partial order and the structural richness on the dynamic heterogeneity require further investigations. The exact mechanism of the dynamic facilitation in GBs remains unknown but could be different from that in homogeneously disordered systems. For example, we found a much larger avalanche length scale (up to ~$70r_0$) compared to that in supercooled liquids and glasses (below ~$10r_0$)[37] (r_0 being the first nearest neighbor distance). Furthermore, this work only studied GBs in a single-component system. Adding segregating solutes to the GB core will add a new level of complexity but will also provide a means to control the GB dynamics. While the segregation effect on GB diffusion has been studied[38], the underlying microscopic mechanisms remain unknown.

Finally, even though most GB diffusion measurements are performed on time and space scales far exceeding the avalanche scales, one should explore alternative methods capable of extracting at least some mechanistic information. For example, isotope effect measurements provided evidence for collective diffusion mechanisms in metallic glasses[39]. Although such measurements do not give detailed information about specific mechanisms and are limited to elements with available isotopes, their application to GB diffusion could still be attempted to confirm the existence of collective atomic rearrangements predicted by the simulations. Dielectric spectroscopy methods have also been used in specific glasses and supercooled liquids to resolve the characteristic frequencies of slow and fast processes during glassy dynamics[40–42]. They, too, could potentially be used to gain at least some insights into the GB diffusion dynamics on the atomic level.

Methods

The Large-scale Atomic/Molecular Massively Parallel Simulator (LAMMPS)[43] was used to conduct molecular statics and MD simulations. The software package OVITO[44] was used for visualization and analysis of the collective diffusion mechanisms. The Al-M and Al-99 potentials were downloaded from the LAMMPS interatomic potential library. The GitHub codes from[45] were used for LAMMPS simulations with the Al-PINN potential.

GB structure optimization. Unrelaxed GB structures were created by joining two grains in a simulation box with periodic boundary conditions in the GB plane (x–y coordinate plane) and free-surface boundary conditions normal to the GB (z-direction). The GB cross-section was chosen with dimensions at least 10 nm by 10 nm in the x and y directions, and each grain had a thickness of at least 6 nm. To study finite-size effects on diffusion, several GB cross-sections were tested up to 32 nm by 32 nm. For the commensurate GBs (Table 1), the lateral bicrystal dimensions were chosen with integer repeats of the coincident site lattice (CSL) unit cell. For the incommensurate GB, the misfit strain was minimized within the maximum interface size (30 nm by 30 nm) and applied to the upper grain only. The minimization procedure was repeated at different temperatures for lattice constants expanded by the precomputed bulk thermal expansion coefficients. The maximum absolute value of the misfit strain used in this work was 1.001.

The initial GB structures were optimized by a standard grid search that seeks to find a deep local energy minimum[46,47]. Several hundred initial unrelaxed GB structures were prepared with different rigid shifts applied to the upper grain relative to the lower. Translations were chosen within a unit cell of the reciprocal lattice of the CSL (known as the displacement shift complete lattice) and included overlaps of the two grains. For each initial structure, pairs of closely spaced atoms were identified and one atom was deleted at random if the overlap radii were in the range 0.7–0.95r_0, where $r_0 = 0.28$ nm is the first nearest neighbor distance in FCC Al. Conjugate gradient minimization was performed at 0 K to relax the atoms in the GB core of each candidate structure. The lowest energy structure was used as input for the subsequent diffusion simulations. This optimization procedure recovered the well-known structures of the Σ3 and Σ17 GBs, but it did not sample different GB densities as in more sophisticated optimization routines[48–50].

Point defect analysis. Wigner-Seitz analysis as implemented in OVITO was used to analyze the point defect content of GBs. This method identifies point defects in a finite-temperature GB structure relative to the Voronoi tessellation of a defect-free reference structure. As the reference state, we used the 0 K GB structure homogeneously expanded by the thermal expansion coefficient at the chosen temperature. Trajectory smoothing was applied over a time window of O(10) ps to mitigate the effect of thermal noise during defect identification.

GB self diffusion coefficient calculations. GB diffusion was studied by canonical (NVT) and microcanonical (NVE) MD simulations. A multi-step equilibration procedure was performed before production runs. First, the bicrystal was homogeneously expanded by the precomputed bulk thermal expansion strain at the chosen temperature. Next, a 1 nm thick rigid slab at the top of the upper grain was allowed to float in z-direction during a short (0.1 ns) NVT anneal. Combined with the pre-expansion, this step reduced the pressure in the grains to near zero. Then, the rigid slabs at the top and bottom of the bicrystal were fixed and an NVT anneal was performed for 1 ns. The fixed boundary conditions suppressed spontaneous GB sliding events to clearly identify the diffusion mechanisms. After the equilibration, production NVT runs were performed for up to 40 ns and several hundred dump files were output for the subsequent calculation of the diffusion coefficients. NVE simulations were then performed starting from the end of each NVT run to analyze the diffusion mechanisms. The NVE ensemble was chosen to eliminate any possible effect of the thermostat on spontaneous diffusive events. For selected calculations, including diffusion measurements at low temperatures, additional statistics were obtained by performing multiple runs with different velocity seeds.

The GB self-diffusion coefficients were measured by tracking atoms within a 2 nm thick layer centered at the GB. The current GB position was determined as the average z-coordinate of non-FCC atoms identified by the polyhedral template matching modifier in OVITO[51]. The diffusion coefficients within the layer were calculated from the Einstein relations $D_x = \langle x^2 \rangle / 2t$ and $D_y = \langle y^2 \rangle / 2t$, where $\langle x^2 \rangle$ and $\langle y^2 \rangle$ are the MSDs of atoms in the respective directions parallel to the GB plane and t is the simulation time. Bootstrap resampling was employed as in[52] to compute error estimates associated with the diffusion coefficient. The hyperparameters chosen for this method include a smoothing window of 5 ps, a block length of 20 ps, and the number of resampled trajectories equal to 100. Note that using a fixed-width layer can underestimate the diffusion coefficient because of the possible inclusion of some of the immobile atoms from the perfect lattice regions next to the GB core. This underestimation was corrected by rescaling the diffusion coefficients by the average inverse fraction of the mobile atoms in the layer at long times. The convergence of diffusion calculations in time was verified by checking

that the slope of the log(MSD)-log(t) plot was equal to one. All diffusion coefficients reported here satisfied this condition.

At high temperatures (typically, $T > 0.85T_m$) and depending on the GB, random interface displacements were observed in addition to diffusion. When the average interface position changed by more than 0.5 nm, the diffusion calculation was reset from the new GB position.

Liquid self diffusion coefficient calculations. To compute the liquid diffusion coefficients, an initial 32,000-atom liquid structure was created in a periodic box by heating a perfect Al crystal in the isothermal-isobaric (NPT) ensemble to 1500 K and holding it for 200 ps. Next, a set of liquid samples was generated in the temperature range from 1050 to 1450 K by quenching the high-temperature structure at a rate of 50 K/100 ps and holding it at the set temperature for 200 ps. A further stepwise quenching was performed from 1050 K to 600 K at a rate of 25 K/ns with a hold time of 2 ns every 50 K. These times were sufficient for liquid equilibration at the chosen temperatures as evidenced by converged total potential energy and linear MSD vs time behavior. Crystallization was observed at and below 650 K, and these temperatures were not used for the diffusion calculations. Production NVE anneals were performed for all liquid structures for 0.1 ns. The diffusivity was computed from the 3D Einstein relation $D = \langle r^2 \rangle / 6t$ and averaged over 20 independent runs with different velocity seeds.

Analysis of hierarchical time and length scales associated with diffusion avalanches. The following algorithm was used to reveal string-like displacements in GB diffusion. First, mobile atoms were identified within the GB core such that the net displacement of an atom Δr during a preset time interval Δt was within the range $0.4r_0 < \Delta r < 1.2r_0$. Here, the upper bound was chosen to eliminate atoms that had undergone multiple hops, and the lower bound was chosen to eliminate immobile atoms. Next, mobile atomic pairs (i, j) were found that remained nearest neighbors at the times $t = 0$ and $t = \Delta t$ and satisfied the criterion $\min(|r_i(t) - r_j(0)|, |r_j(t) - r_i(0)|) < 0.43r_0$. This criterion captures atomic pairs with string-like motion in which one atom jumps into the previous position of the other. The algorithm has three hyper-parameters: the lower and upper bounds for the displacement and the substitution distance (the multiplicative factors 0.4, 1.2 and 0.43 above). These parameters were chosen based on the prior studies of diffusion in glass-forming supercooled liquids[8,11] and were fixed across all GBs studied in this work.

All mobile pairs containing common atoms were then joined into larger string-like clusters, and each cluster was assigned a unique ID. Cluster statistics were then computed over all clusters, including the number of atoms and the gyration tensor. The string identification algorithm was repeated for a range of time intervals Δt with multiple start times. The average string length, measured by the average number of atoms in the string-like cluster, typically exhibits a single maximum as a function of Δt at a characteristic time $\Delta t = t_s^*$.

The analysis of diffusion avalanches required a more flexible definition of mobile clusters. The input to this method is the space-time trajectory consisting of atomic displacement fields computed at a fixed time interval (Δt) and stacked in time. Here, Δt is a hyper-parameter taken to be approximately $0.02t_s^*$. First, the string clustering step was performed in space-time with no upper bound on the displacement length and all other hyper-parameters as above. The lack of an upper bound allows the strings to incorporate atoms executing multiple jumps. Next, the string connectivity criterion was relaxed: neighboring strings were combined in space if at least two atoms in adjacent strings (either in time or space) were no more than $1.2r_0$ apart. This hyper-parameter can be interpreted as a cutoff distance for the interaction range in dynamic facilitation. It also provides a good visual segmentation of the data. If the cutoff distance is too large, or the trajectories in space-time are too dense, then all atoms are part of the same mobile cluster and the algorithm loses its meaning. In the space-time trajectories, the same atom can be included multiple times in the same mobile cluster if it executes multiple jumps. The mobile clusters often form elongated, anisotropic shapes in space-time. Their size was quantified as the number of unique atoms in the cluster. The dynamic length scale of a given mobile cluster was quantified as its maximum width along a given direction in the GB plane, and its timescale as the maximum width along the time axis.

Immobile clusters are also apparent in space-time diagrams as empty regions (bubbles[24]) separating the mobile clusters. In principle, their length and time scales can be computed in a similar manner as for the mobile clusters. However, in practice a single percolating immobile cluster in the space-time diagram is often found with this method. An alternative method used here defines and computes the immobility time by considering individual square ($l \times l$) GB patches in space. The immobility time in each patch is then computed as the time between mobility events. The immobility time scale is obtained in the limit of l approaching zero, while the immobility time distribution can be computed at $l = r_0$. The ratio of the immobility and mobility times can also serve as a measure of diffusion intermittency. Considered as a function of the patch size l, this ratio is used in the virtual size-effect tests as shown in Supplementary Fig. 2.

Data availability

The data supporting the findings of this study are available in the Supplementary Information file or from the corresponding authors upon reasonable request. The computer simulation part of this research used the publicly available codes LAMMPS and OVITO. The routine computer scripts controlling the execution of the calculations are not central to this work but are available from the corresponding authors upon reasonable request.

Code availability

The code for computer simulations and post-processing analysis of avalanche-like diffusion mechanisms is available upon reasonable request.

Received: 17 August 2022; Accepted: 31 October 2022;
Published online: 12 November 2022

References

1. Sutton, A. P. & Balluffi, R. W. *Interfaces in Crystalline Materials* (Clarendon Press, Oxford, 1995).
2. Kaur, I. Mishin, Y. & Gust, W. *Fundamentals of Grain and Interphase Boundary Diffusion* (Wiley, Chichester, West Sussex, 1995).
3. Mishin, Y., Asta, M. & Li, J. Atomistic modeling of interfaces and their impact on microstructure and properties. *Acta. Mater.* **58**, 1117–1151 (2010).
4. Sørensen, M. R., Mishin, Y. & Voter, A. F. Diffusion mechanisms in cu grain boundaries. *Phys. Rev. B* **62**, 3658 (2000).
5. Suzuki, A. & Mishin, Y. Atomistic modeling of point defects and diffusion in copper grain boundaries. *Interface Sci.* **11**, 131–148 (2003).
6. Suzuki, A. & Mishin, Y. Atomic mechanisms of grain boundary diffusion: Low versus high temperatures. *J. Mater. Sci.* **40**, 3155–3161 (2005).
7. Mishin, Y. An atomistic view of grain boundary diffusion, in: Defect and Diffusion Forum, volume 363, Trans Tech Publ, 2015, pp. 1-11.
8. Zhang, H., Srolovitz, D. J., Douglas, J. F. & Warren, J. A. Grain boundaries exhibit the dynamics of glass-forming liquids. *Proc. Natl Acad Sci.* **106**, 7735–7740 (2009).
9. Donati, C. et al. Stringlike cooperative motion in a supercooled liquid. *Phys. Rev. Lett.* **80**, 2338 (1998).
10. Derlet, P., Bocquet, H. & Maaß, R. Viscosity and transport in a model fragile metallic glass. *Phys. Rev. Mater.* **5**, 125601 (2021).
11. Zhang, H., Wang, X., Yu, H.-B. & Douglas, J. F. Dynamic heterogeneity, cooperative motion, and Johari–Goldstein β relaxation in a metallic glass-forming material exhibiting a fragile-to-strong transition. *Eur. Phys. J. E* **44**, 1–30 (2021).
12. Fransson, E. & Erhart, P. Defects from phonons: Atomic transport by concerted motion in simple crystalline materials. *Acta. Mater.* **196**, 770–775 (2020).
13. Annamareddy, A. & Eapen, J. Low dimensional string-like relaxation underpins superionic conduction in fluorites and related structures. *Sci. Rep.* **7**, 1–12 (2017).
14. Saylor, D. M., El Dasher, B. S., Rollett, A. D. & Rohrer, G. S. Distribution of grain boundaries in aluminum as a function of five macroscopic parameters. *Acta. Mater.* **52**, 3649–3655 (2004).
15. Mendelev, M., Kramer, M., Becker, C. A. & Asta, M. Analysis of semi-empirical interatomic potentials appropriate for simulation of crystalline and liquid Al and Cu. *Philos. Magaz.* **88**, 1723–1750 (2008).
16. Medlin, D., Mills. M., Stobbs, W., Daw, M. & Cosandey F. HRTEM observations of a $\Sigma = 3\{112\}$ bicrystal boundary in aluminum, MRS Online Proceedings Library (OPL) 295 (1992).
17. Medlinet, D. et al. Migration dynamics of a $\Sigma = 3\{112\}$ boundary in aluminum, MRS Online Proceedings Library (OPL) 319 (1993).
18. Wang, J., Misra, A. & Hirth, J. Shear response of $\Sigma = 3\{112\}$ twin boundaries in face-centered-cubic metals. *Phys. Rev. B* **83**, 064106 (2011).
19. Marquis, E., Hamilton, J., Medlin, D. & Léonard, F. Finite-size effects on the structure of grain boundaries. *Phys. Rev. Lett.* **93**, 156101 (2004).
20. Koju, R. & Mishin, Y. Atomistic study of grain-boundary segregation and grain-boundary diffusion in Al-Mg alloys. *Acta. Mater.* **201**, 596–603 (2020).
21. Hooshmand, M. S., Zhong, W., Zhao, J. C., Windl, W. & Ghazisaeidi, M. Data on the comprehensive first-principles diffusion study of the aluminum-magnesium system. *Data in Brief* **30**, 105381 (2020).
22. Hickman, J. & Mishin, Y. Disjoining potential and grain boundary premelting in binary alloys. *Phys. Rev. B* **93**, 224108 (2016).
23. Jung, Y., Garrahan, J. P. & Chandler, D. Dynamical exchanges in facilitated models of supercooled liquids. *J. Chem. Phys.* **123**, 084509 (2005).
24. Chandler, D. & Garrahan, J. P. Dynamics on the way to forming glass: Bubbles in space-time. *Annu. Rev. Phys. Chem.* **61**, 191–217 (2010).
25. Foiles, S. & Hoyt, J. J. Computation of grain boundary stiffness and mobility from boundary fluctuations. *Acta Mater.* **54**, 3351–3357 (2006).
26. Mendelev, M. I. et al. Development of new interatomic potentials appropriate for crystalline and liquid iron. *Philos. Magaz.* **83**, 3977–3994 (2003).

27. Olmsted, D., Foiles, S. & Holm, E. A. Survey of computed grain boundary properties in face-centered cubic metals: I. Grain boundary energy. *Acta. Mater.* **57**, 3694–3703 (2009).
28. Ratanaphan, S. et al. Grain boundary energies in body-centered cubic metals. *Acta. Mater.* **88**, 346–354 (2015).
29. Mishin, Y., Farkas, D., Mehl, M. & Papaconstantopoulos, D. Interatomic potentials for monoatomic metals from experimental data and ab initio calculations. *Phys. Rev. B* **59**, 3393 (1999).
30. Pun, G. P., Yamakov, V., Hickman, J., Glaessgen, E. & Mishin, Y. Development of a general-purpose machine-learning interatomic potential for aluminum by the physically informed neural network method. *Phys. Rev. Mater.* **4**, 113807 (2020).
31. Starikov, S., Mrovec, M. & Drautz, R. Study of grain boundary self-diffusion in iron with different atomistic models. *Acta Mater.* **188**, 560–569 (2020).
32. Pan, A. C., Garrahan, J. P. & Chandler, D. Heterogeneity and growing length scales in the dynamics of kinetically constrained lattice gases in two dimensions. *Phys. Rev. E* **72**, 041106 (2005).
33. Schönfelder, B., Gottstein, G. & Shvindlerman, L. Comparative study of grain-boundary migration and grain-boundary self-diffusion of [0 0 1] twist-grain boundaries in copper by atomistic simulations. *Acta. Mater.* **53**, 1597–1609 (2005).
34. Eduardo, S. et al. Avalanches mediate crystallization in a hard-sphere glass. *Proc. Natl Acad. Sci.* **111**, 75–80 (2014).
35. Koch, R. H., LLoyd, J. R. & Cronin, J. 1/f noise and grain-boundary diffusion in aluminum and aluminium alloys. *Phys. Rev. Lett.* **55**, 2487 (1985).
36. Zhang, H. & Douglas, J. Glassy interfacial dynamics of Ni nanoparticles: part I Colored noise, dynamic heterogeneity and collective atomic motion. *Soft Matter* **9**, 1254–1265 (2013).
37. Royall, C. P. & Williams, S. R. The role of local structure in dynamical arrest. *Phys. Rep.* **560**, 1–75 (2015).
38. Koju, R. K. & Mishin, Y. Relationship between grain boundary segregation and grain boundary diffusion in Cu-Ag alloys. *Phys. Rev. Mater.* **4**, 073403 (2020).
39. Faupel, F. et al. Diffusion in metallic glasses and supercooled melts. *Rev. Mod. Phys.* **75**, 237 (2003).
40. Lunkenheimer, P. & Loidl, A. Dielectric spectroscopy of glass-forming materials: α-relaxation and excess wing. *Chem. Phys.* **284**, 205–219 (2002).
41. Jug, G., Loidl, A. & Tanaka, H. On the structural heterogeneity of supercooled liquids and glasses (a). *EPL (Europhys. Lett.)* **133**, 56002 (2021).
42. Arceri, F., Landes, F., Berthier, L. & Biroli, G. A statistical mechanics perspective on glasses and aging, arXiv:2006.09725, 2022.
43. Plimpton, S. Fast parallel algorithms for short-range molecular dynamics. *J. Comput. Phys.* **117**, 1–19 (1995).
44. Stukowski, A. Visualization and analysis of atomistic simulation data with OVITO–the open visualization tool. *Modelling Simul. Materi. Sci. Eng.* **18**, 015012 (2009).
45. Files for running PINN simulations in LAMMPS: https://github.com/ymishin-gmu/LAMMPS-USER-PINN.
46. Olmsted, D. L., Holm, E. A. & Foiles, S. M. Survey of computed grain boundary properties in face-centered cubic metals. II: Grain boundary mobility. *Acta. Mater.* **57**, 3704–3713 (2009).
47. Tschopp, M. A., Coleman, S. P. & McDowell, D. L. Symmetric and asymmetric tilt grain boundary structure and energy in Cu and Al (and transferability to other fcc metals). *Integr. Mater. Manuf. Innov.* **4**, 11 (2015).
48. Frolov, T., Olmsted, D. L., Asta, M. & Mishin, Y. Structural phase transformations in metallic grain boundaries. *Nat. Comm.* **4**, 1–7 (2013).
49. Hickman, J. & Mishin, Y. Extra variable in grain boundary description. *Phys. Rev. Mater.* **1**, 10601 (2017).
50. Yang, C., Zhang, M. & Qi, L. Grain boundary structure search by using an evolutionary algorithm with effective mutation methods. *Comput. Mater. Sci.* **184**, 109812 (2020).
51. Larsen, P. M., Schmidt, S. & Schiøtz, J. Robust structural identification via polyhedral template matching. *Modelling Simul. Mater. Sci. Eng.* **24**, 055007 (2016).
52. Race, C. Quantifying uncertainty in molecular dynamics simulations of grain boundary migration. *Mol. Simul.* **41**, 1069–1073 (2015).
53. Zhong, W., Hooshmand, M. S., Ghazisaeidi, M., Windl, W. & Zhao, J.-C. An integrated experimental and computational study of diffusion and atomic mobility of the Aluminum–Magnesium system. *Acta. Mater.* **189**, 214–231 (2020).
54. Dais, S., Messer, R. & Seeger, A. Nuclear-magnetic-resonance study of self-diffusion in aluminium, in: Materials Science Forum, volume 15, Trans Tech Publ, 1987, pp. 419-424.

Acknowledgements

We would like to thank Raj Koju, Jack Douglas and Peter Derlet for helpful discussions. This research was supported by the National Science Foundation, Division of Materials Research, under Award no. 2103431.

Author contributions

Y.M. acquired funding for this research. I.C. wrote all computer codes/scripts required for this work and conducted all simulations reported here under Y.M.'s guidance and supervision. Both authors participated equally in interpreting the results and writing the paper, and approved its final version.

Competing interests

The authors declare no competing interests.

Additional information

Supplementary information The online version contains supplementary material available at https://doi.org/10.1038/s43246-022-00314-7.

Correspondence and requests for materials should be addressed to Ian Chesser or Yuri Mishin.

Peer review information *Communications Materials* thanks Sergei Starikov, Snehanshu Pal and Daniel Utt for their contribution to the peer review of this work. Primary Handling Editors: Jet-Sing Lee and John Plummer. Peer reviewer reports are available.

Reprints and permission information is available at http://www.nature.com/reprints

Publisher's note Springer Nature remains neutral with regard to jurisdictional claims in published maps and institutional affiliations.